Hindawi
Journal of Engineering
Volume 2022, Article ID 1796876, 10 pages
https://doi.org/10.1155/2022/1796876

Research Article

Effect of Interlayer Stress on U Bends and Water Droplet Bends

Qiujun Wang,[1] **Weiwei Su**,[1] **Wenxin Zhang**,[1] **Zeyu Zhang**,[1] **Bo Wang**,[1] **Di Zhang**,[1] **and Fang Zhang**[2]

[1]*Hebei Key Laboratory of Flexible Functional Materials, School of Materials Science and Engineering, Hebei University of Science and Technology, Shijiazhuang 050021, China*
[2]*Yungu (Gu'an) Technology Co., Ltd, Langfang 065500, China*

Correspondence should be addressed to Bo Wang; wangbo1996@gmail.com

Received 3 May 2022; Revised 9 July 2022; Accepted 9 August 2022; Published 20 September 2022

Academic Editor: Francesco Tornabene

The interlayer stress (IS) analysis of the flexible active-matrix organic light-emitting diode (AMOLED) panel is critical for decreasing the stress concentration and reducing the risk of overall screen failure. This article relies on the linear elastic models of ABAQUS to simulate finite element analysis of foldable panels. This article discussed three sensitive locations of the flexible AMOLED panel caused by two different bending methods including U bends and water droplet bends. The finite element method for simulating the layer analysis was constructed to analyze the effect of optically clear adhesive (OCA) film thickness on the distribution of stress and strain. The module can be optimized by changing the thickness and shear modulus of OCA. With the decrease of OCA thickness and the increase of stiffness, the maximum stress of the organic light-emitting diode (OLED) layer is decreased by 20% which is 55 Mpa; meanwhile, the IS of the entire module is reduced by about 30%.

1. Introduction

With the popularity of smartphones, flat-screen TVs, and laptops, display panels as a core component of electronics are best-in-class development. As the primary way to communicate with people, display performance is critical to the user experience [1]. Japan, South Korea, Taiwan, and China have spent great effort in display technology development. Flexible active-matrix organic light-emitting diodes (AMOLED) with many attractive features, including high resolution, low power consumption, lightweight, and wide viewing angle, have a profound effect on displays [2]. With the continuous development of personal smart terminals, flexible OLED screens offer a wider range of applications. Compared to curved screens and full-screen mobile phones, foldable mobile phones can better meet people's requirements for communication [3]. Breakage and shedding as the common stress problems in folding screens have been bothering and hindering the promotion of the consumer market [4]. The main purpose is to compare and analyze technical solutions for flexible AMOLED display modules. Each functional film layer contains only one layer of first-order solid elements, which will result in a larger calculation error caused by the clipping self-lock effect. Therefore, it is difficult to simulate the transmission of pressure between functional film layers [5]. In this paper, a hyperelastic model of OCA is proposed. The introduction of hyperelastic parameters has the effect of scaling with strain to realize the correlation between the mechanical properties of materials and time [6]. The global pressure and pressure check the distribution of the folding panel [7–10]. Investigate the impact of the stacking structure further. Finally, the paper puts forward some suggestions to optimize the panel structure and operate effectively. The most flexible AMOLED display module folding scheme has been proposed by comparing and studying different laminate bending designs from the aspects of pressure and strain, material, process selection, and simulation optimization [11–13]. The 7-inch flexible AMOLED module is produced by selecting different locations for the film layer and process plan [14, 15]. Reliability, optical, and mechanical testing of the finished screen is carried out through mechanical

Table 1: Material data for each layer of the module.

Panel component	Material	Density (tone/mm^3)	Young's modulus (GPa)	Poisson's ratio	Thickness (μm)
Cover film	PI	1490	6	0.25	56
OCA1	PMMA	1180	0.025	0.475	25
POL	PVA	1290	4	0.33	67
OCA2	PMMA	1180	0.025	0.475	25
Barrier film	PI	1490	3	0.31	20
OLED + TFT + PI	PI	1395	1.6	0.34	20
OCA3	PMMA	1180	0.025	0.475	50
Backplane	PI	1490	3	0.32	75

simulation and testing, and the panel is more effectively prevented from peeling or layering, and test results are given.

2. Model Description

2.1. Geometric Model and Boundary Conditions. The bending process of the collapsible AMOLED panel is simulated as a plane strain problem using nonlinear finite component software ABAQUS. The common hard screen AMOLED module stacking technology mainly involving module optics, mechanics, heat, function, and appearance is very mature. Since stress and strain are associated with elastic modularity, strain is the main consideration. ABAQUS can calculate the change of stress by the elastic module. Modulus considers only the tensile stress during bending, regardless of the effect of shear slip.

The flexible module stack design is mainly based on material process selection, film layer simplification, and simulation for scheme design. At present, the thickness of common polarizers (POL) is basically between 143 and 170 microns and generally includes two parts: linear polarizers and quarter-wave plates. The OLED device material is easily affected by water and oxygen, and its performance will be degraded. Although there is usually a layer of encapsulation on the surface of the OLED screen, in order to further improve its service life and reliability test results, a barrier film (barrier film) will be attached after encapsulation, which is also used to block water and oxygen. The barrier film is usually attached to the top surface of the screen. The thickness of the barrier film is between 50 and 150 microns. It is usually located on the top surface of the display screen to protect the screen. The cover film in the flexible AMOLED screen is similar to the cover glass in the ordinary AMOLED screen, and it is usually located on the uppermost surface of the display screen to protect the screen. The thickness of the protective sheet for flexible AMOLED is between 30 and 90 microns. The whole is a double-sided nonadhesive module material. The support film (back plate film) is usually only used for flexible AMOLED screens because the original glass substrate of the flexible AMOLED screen will be peeled off by laser during the production process, and then the support film will be attached to the other side of the PI substrate to realize the screen body in the production process. In the process of "flexibility," the stress on the upper end is balanced and the mechanical properties of the entire screen are enhanced. The thickness of the supporting film is selected between 50 and 75 microns. The whole is a single-sided adhesive module material.

According to industrial production, the thickness of the OCA layers is 25 μm, 25 μm, and 50 μm, respectively. In addition, the rest of the film materials are simplified as linear elastic materials. Both thickness of each film layer and specific parameters are shown in Table 1.

In the experiment, two auxiliary steel plates were used to bend the flexible screen. In this experiment, a separate module screen was used for the experiment without adding electronic devices. The length of the flexible screen is 146.7 mm, the width is 71.5 mm, the thickness is 338 μm, and the bending radius is 3 mm. We made a 180-degree U bend on the experimental object as shown in Figure 1(b). The steel plate covers a lot of the flexible screen, so it is difficult to see clearly. Figure 1(a) is a schematic diagram of the bending of the flexible screen during the experiment. Since the mechanical properties of the longitudinal section of the flexible screen are the same when it is bent, we used a two-dimensional model to replace the three-dimensional model of the experiment in the simulation. The initial state of the flexible screen and various parameters of the sample are shown in Figure 1(c). The schematic diagram in Figure 1(d) is the state and movement of the flexible screen after the U-shaped bending is completed. There are auxiliary instruments on both sides to finish.

The coupling of the two reference points is set on both sides of the midpoint of the module, which drives the module to rotate. To form an arc shape when bending, the bending part will reduce the stress on the structure. The distance between the reference point and the axis of symmetry is πR/2 mm. When $R = 3$ mm, the distance is 4.71 mm. The structure and schematic diagram are shown in Figure 2. The coupled reference point RP-1 rotates clockwise at a speed of 1.57 rad/s and moves to the right at $(\pi/2)$ R mm/s simultaneously. The figure after bending is shown in Figure 2(b), followed by static Set 300 s to simulate actual usage.

2.2. Elastic Properties of Orthotropic Materials. The Mooney–Rivlin model is based on rubber isotropy and approximate incompressible volume assumption. In engineering, the strain energy density function is generally

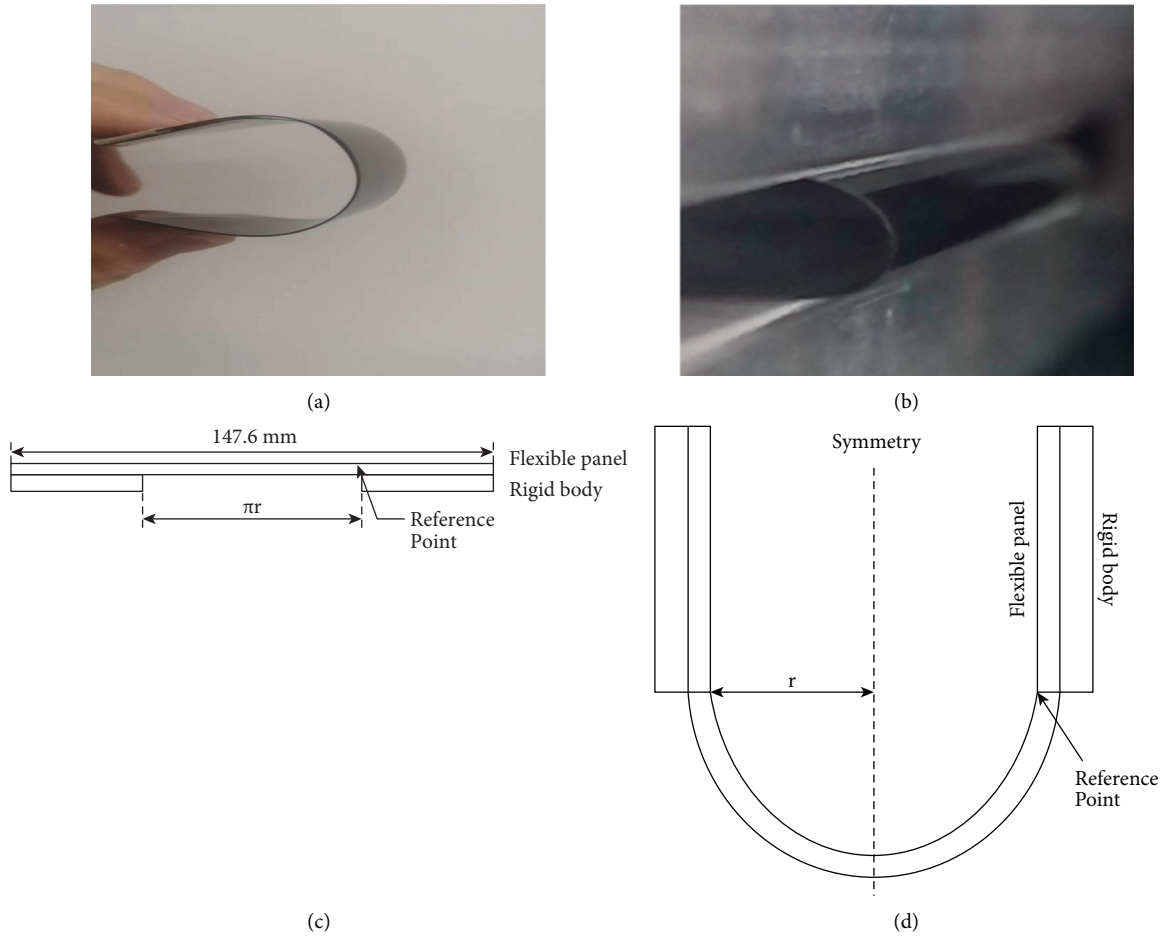

Figure 1: (a) Schematic diagram of U-shaped bending of the flexible screen. (b) Flexible screen U-shaped experimental bending diagram. (c) Schematic representation of the model before folding. (d) Schematic diagram of the model after folding.

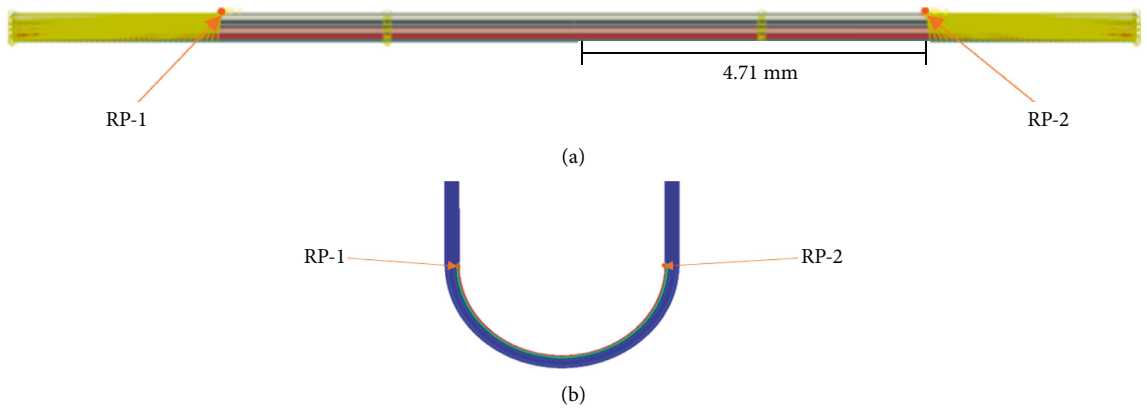

Figure 2: (a) Before the module is bent. (b) After the module is bent. Composite lamina.

used for rubber to characterize the superelasticity of the material. The polynomial strain energy function in the analysis has been more widely used in finite element analysis [16]. For rubber in terms of similar incompressible physical nonlinear materials, the Mooney–Rivlin strain energy function is the most common choice. Its constitutive relationship is as follows [17]:

$$U = \sum_{i+j=1}^{N} C_{ij} (I_1 - 3)^i (I_2 - 3)^j + \sum_{i=1}^{N} \left[\left(\frac{1}{D_i} \right) (J-1)^{2i} \right], \quad (1)$$

$$I_1 = \lambda_1^2 + \lambda_2^2 + \lambda_3^2,$$

$$I_2 = (\lambda_1 \lambda_2)^2 + (\lambda_2 \lambda_3)^2 + (\lambda_3 \lambda_1)^2.$$

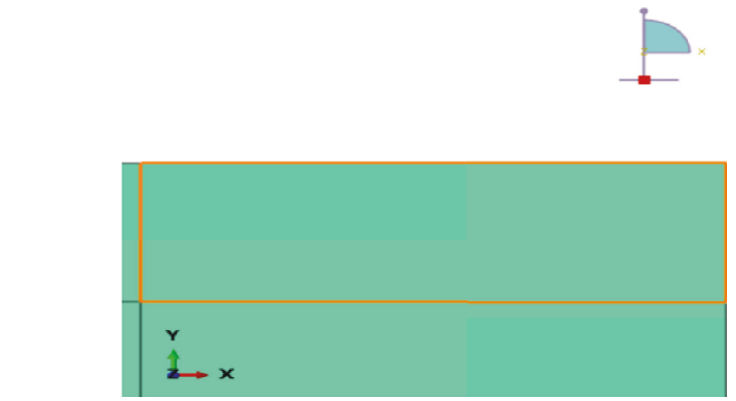

(a)

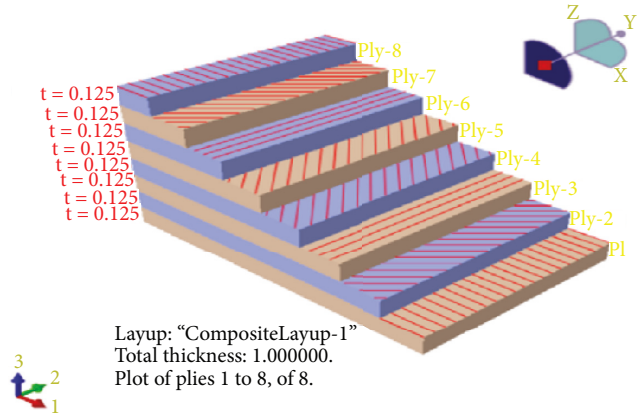

(b)

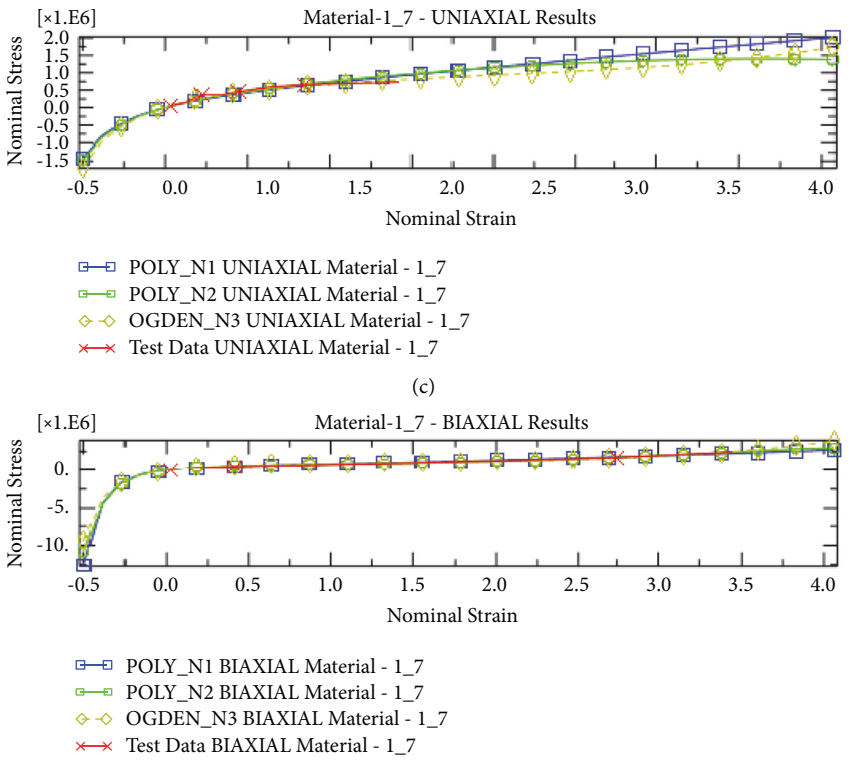

(c)

(d)

Figure 3: Continued.

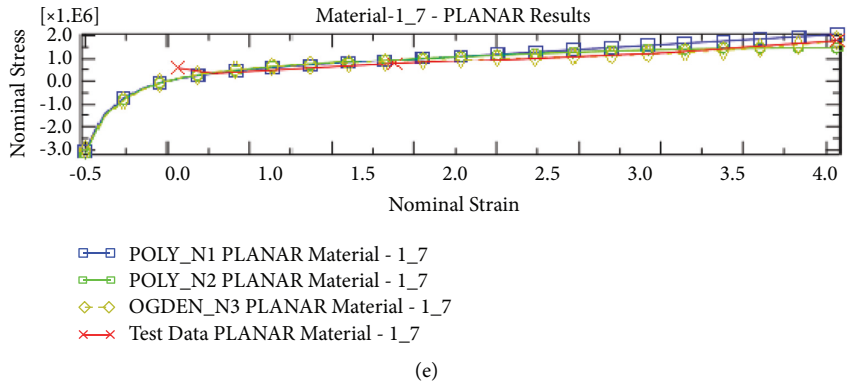

(e)

Figure 3: Composite lamina (a) and laminate (b). (c) Uniaxial tensile test date. (d) Test biaxial tensile test date. (e) Plane tensile test date.

U is the strain energy density; N is the class of the function; C_{ij} is a material constant, usually obtained by experimental tests; I_1 and I_2 are the first-order and the second-order strain invariants [18, 19]; D_i is the material constant, which is related to the pressure of the material shrinkage correlation; J is the volume; and λ_3 are the main extension rate [20]. Based on the above constitutive relationship, the strain energy function of the incompressible material is established and is as follows:

$$U = C_{10}(I_1 - 3) + C_{01}(I_2 - 3) + \frac{1}{D_1(J-1)^2}. \quad (2)$$

C_{10} and C_{01} are the material constants obtained from the experiment, and D_1 is the material constant and is related to the compressibility of the material. Studies have shown that the Mooney–Rivlin model is a superelastic model type, which can better simulate the application of rubber materials' time-changing characteristics. The OCA hyperelastic model in this article is used in the simulation. To get more reliable superelastic parameters of OCA, we did a uniaxial tensile test and biaxial tensile and plane tensile test OCA to determine the parameters of OCA in the Mooney–Rivlin model as shown in Figures 2(c)–2(e).

The single-layer board presents orthotropic anisotropy on a macroscopic scale. As shown in Figure 3, the direction parallel to the fiber of the single-layer board is called the longitudinal direction (or 1 direction), and the direction perpendicular to the fiber is called the transverse direction, along the thickness direction is 3 directions [20]. Generally, materials can show the strongest performance along the longitudinal direction, while the performances along the transverse and thickness directions are low and approximately equal.

2.3. Meshing and Accuracy Verification. In this paper, the implicit dynamic viscoelastic analysis step has been used for analysis and calculation. To be consistent with the real force, plane strain grids have been applied in this model. When dividing the grid, quadrilateral grids are used to facilitate convergence and calculation.

In the thickness direction, all membrane materials and OCA adhesive materials are divided into three layers. The grid-type used in this paper is plane strain, hybrid, and reduced integral CPE8RH element. The accuracy of meshing usually affects the accuracy of the results. Generally speaking, the finer the meshing is, the more accurate the result will be. However, if the mesh is too dense, the computational overhead and the calculation time will increase obviously. For display dynamics algorithms, computer memory consumption and calculation time consumption are proportional to the number of grid cells. The computational cost increases with the increase in the fineness of the grid division. It can be more directly predicted that the grid refinement will cause cost changes. But for the implicit dynamics algorithm used in this article, the computer memory consumption and computing time consumption will have an exponential relationship with the number of grid cells. Therefore, using a reasonable mesh density can greatly optimize the calculation cost the same with the same accuracy to verify whether the mesh density of the current model can meet the accuracy requirements, a more refined model is used for the comparison of calculation results. The original model is in the length direction, and the grid size is 0.025 mm. In the thickness direction, all layers are divided into 3 layers. We use the implicit viscoelastic analysis step to reduce the calculation time and reduce the probability of grid distortion. Each film layer is divided from three layers to six layers to transmit longitudinal stress to reduce the value of residual stress. We also changed the mesh size to reduce the mesh size without losing experimental data and without increasing the simulation time, minimizing the error caused by mesh errors on the simulation. The results of partial model division are shown in Figure 4. For comparison, the refined model is used in the length direction, and the grid size is 0.0125 mm. In the thickness direction, all layers are divided into 6 layers, and the results of partial model division are shown in Figure 4.

Since the full integration unit may have a shear self-locking problem, the commonly used eight-node hexagonal contraction overall reduction unit is C3D8R. The appropriate element type, the secondary reduction, and integration element C3D20R are determined by comparing the influence of stress on IS. Figure 4 shows each lamination sequence. When each functional film layer is divided into 3 layers of grid cells, the stresses of the three layers of grid cells

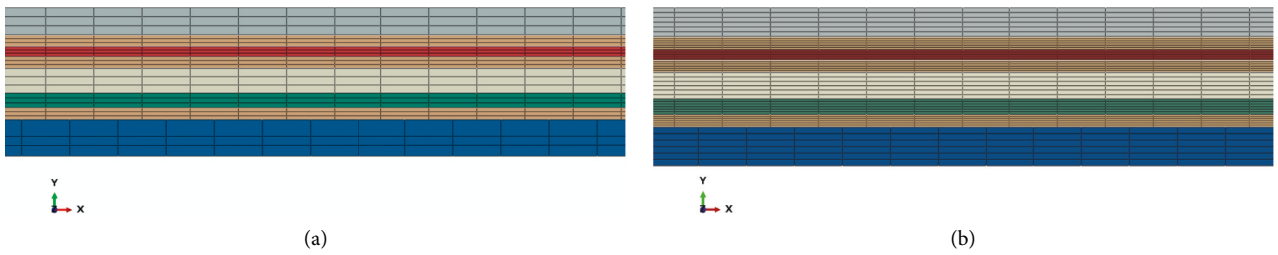

(a) (b)

Figure 4: Part of the mesh in the panel: (a) default mesh and (b) refined mesh.

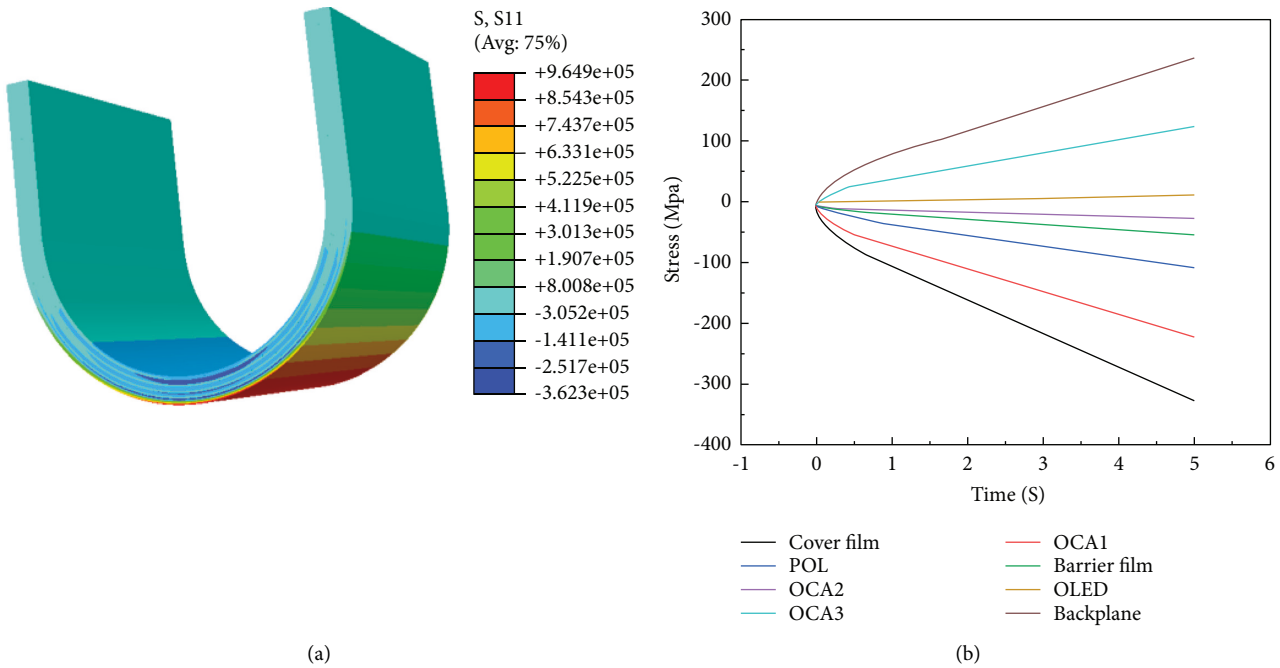

(a) (b)

Figure 5: Stress changes for each film layer during U-shaped bending (a) show the end of module bending. (b) U-shaped bending pressure graph of each module over time.

are superimposed along the thickness direction. The neutral layer represents the integrity of the grid layer stress of the membrane layer.

2.4. Global Stress and Strain Distribution in Folding Panels. During the U-shaped bending, the bending stress of each film layer changes proportionally with time, as shown in Figure 5.

As shown in Figure 5(a), the distribution of cloud images in each field shows a certain symmetry. Among them, the displacement field cloud distribution with only some angle changes is clear and stable. It can be seen that the displacement field in the x-direction is approximately symmetrical with the y-axis. Cloud images change rapidly at the beginning of loading. When the tensile displacement of the module reaches about 5 mm, the cloud image begins to form a stable distribution. Figure 5(b) shows the stress changes of the eight functional film layers in the process of stretching and compression. The cover film layer and the backplane bear the greatest tensile pressure, which is also in line with our design of the two functional film layers in the flexible screen. Based on the above, it can be seen that because the cover film is far from the display layer, the buffering effect of the OCA glue layer and the effect of the thickness change on the display area can be ignored. The backplane is closer to the display layer when the thickness changes. It will affect the strain of the display area so that the maximum compressive strain will increase, the maximum tensile strain will decrease, and the device will be damaged. When the strain of the OCA adhesive layer rises, the risk of adhesive layer peeling increases as well.

Therefore, the authenticity of the simulation can be verified. The maximum stress of the Backplane layer reaches 357 MPa, which shows that the risk of failure is also in the backplane layer, and the strength of the backplane should be improved during production. During the bending process, it can be reasonably assumed that the upper part of the screen body is compressed when the lower part is stretched.

3. Results and Discussion

3.1. Fold Multiple Neutral Planes in the Panel. When the flexible display module is in a bent state, the most important thing is to ensure the integrity of the brittle TFT layer, above the PI substrate, and the easily debonded organic light-

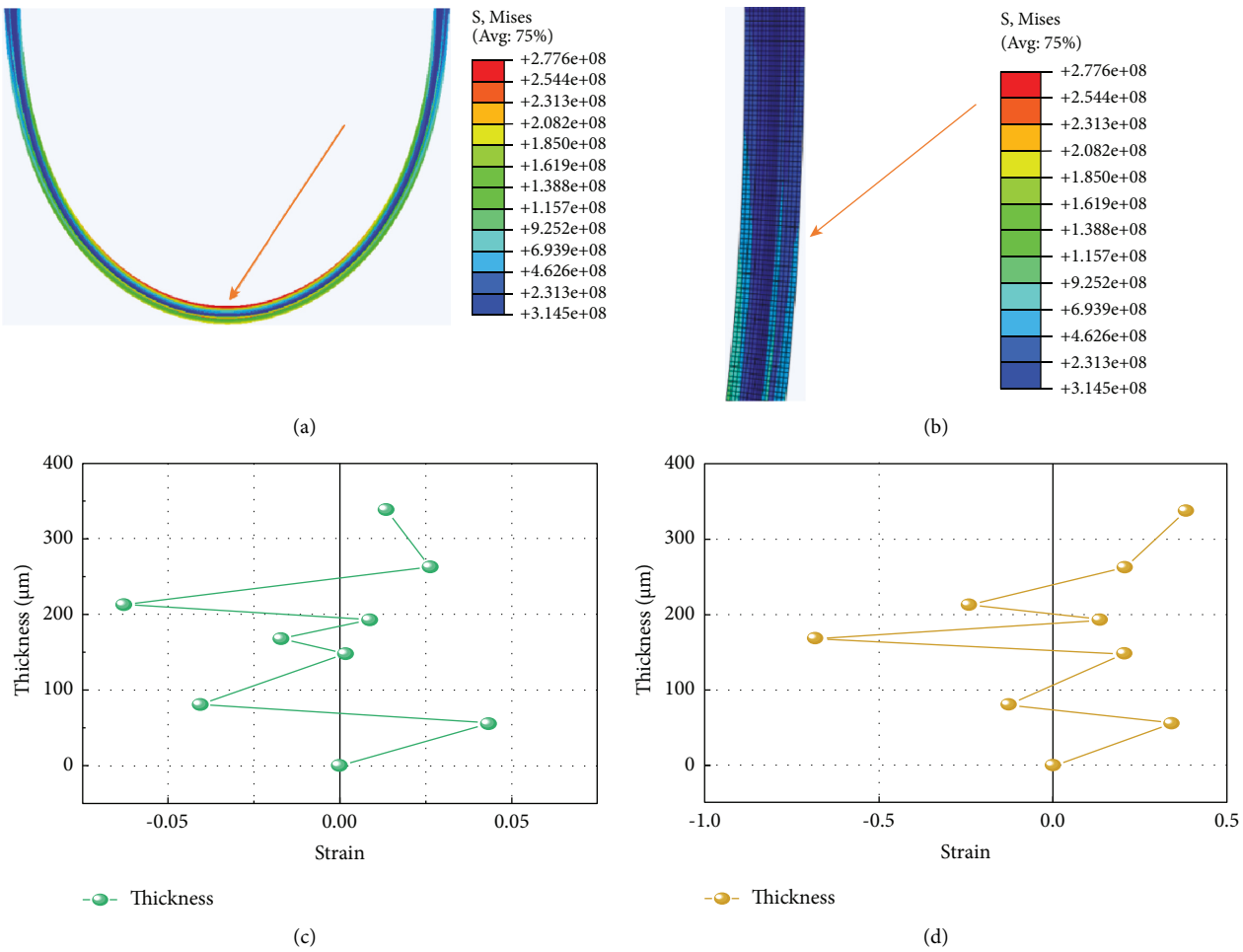

Figure 6: The stress (a) and thickness (c) of the bending area in the U-shaped bend; the tensile stress (b) and the thickness (d) at the end of the u bending area.

emitting layer. There are multiple neutral layer positions (the x-coordinate is equal to 0) in the lamination structure because OCA has a very small elastic modulus compared with the adjacent film layer, resulting in a shielding effect. When the influence between the two layers becomes weak, the structural relationship between the two neutral layers can be analyzed independently. It is vital to keep the position nearing the neutral layer of the module. It is usually achieved by changing the type and thickness of the laminated materials to adjust the position of the neutral layer or to manufacture multiple neutral layers.

In this section, the neutral surfaces in the folding panel and the effect of tensile stress on the panel were examined. The locations where the maximum tensile stress is generated at the three U-shaped bends are also the areas with the most serious fatigue fracture. In Figure 6(d), the tensile stress of the pet rear plane and the POL film layer is maximum, and the deformation on the X-axis is the largest. The tensile force between them and the upper and lower film layers is in a dangerous state.

In Figure 7, the cover film and touch panel have the highest tensile force. When the interface between layers of the same type is located at different thickness locations, the distribution trend of IS is similar, but the magnitude is different. In addition, the magnitude and distribution of normal stress between layers are very different, especially the angle corresponding to the peak value also has a certain deviation. However, the magnitude and distribution of interlayer shear stress are almost the same.

The difference in position of the interface in the x-direction of the same layer does not affect the distribution trend of IS, but only its size and thickness corresponding to the peak value. Among them, IS is greatly affected, and interlayer shear stress is slightly affected. Then explore the relationship between the size of normal stress in the S22 direction and thickness and neutral layer.

As can be seen from Figure 7, the IS on both sides of y-0 changes in the same pattern with the thickness of 193 nm as the dividing line. The size of the dividing line is the same on both sides of the line, but the size of τ_z and τ_x is different, which is related to the laying characteristics and boundary conditions of laminates. Because laminates are centrally symmetrical in the plane, the change of the stratification stresses is the same on both sides of the dividing line. In addition, when the fixed constraints are applied to one end of the laminate and the stretch load is applied to the other

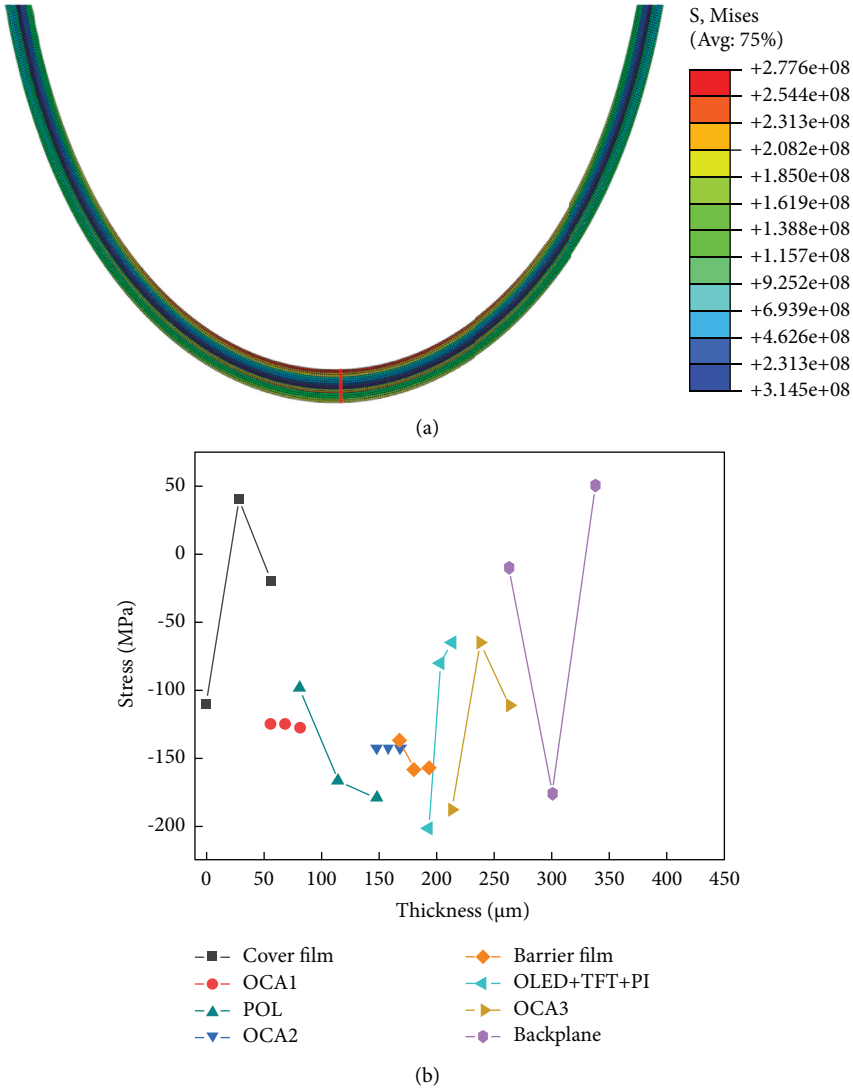

Figure 7: (a) The left is a cloud map of normal stress changes and a thickness map of stress changes. (b) The left half of each number is compression stress, and the right half is the stretch stress.

end of the plane, the stress difference between the layers on both sides of the dividing line will occur.

For the distribution of stress in the subsequent layer, only the part on the other side of the y-0 needs to be studied. As can be seen from Figure 7, when the interface between layers of the same type is located at different thickness locations, the distribution trend of IS is similar, but the magnitude is different. The magnitude and distribution of the normal stress between the various layers are very different, especially the angle corresponding to the peak value also has a certain deviation. Moreover, the value of the transverse strain of the film grid does not change appearance, and the magnitude and distribution of the interlaminar shear stress are almost the same. Therefore, the differences in interface positions between layers along the same thickness direction do not affect the distribution trend of IS, but only their size and the angle corresponding to the peak value. Thus, the force will be greatly affected, while the shear stress between the pull skins is also slightly affected.

3.2. Interlayer Stress. The maximum stress of the module is located in the bending zone, reaching 705 MPa. It usually has good mechanical properties along the fiber direction, while the mechanical properties perpendicular to the fiber direction mainly depend on the properties of the matrix material and the bonding ability of the matrix and the fiber. Due to the bending curvature of the entire module, the maximum stress of S22 is on the backplane of the module. From Figure 8, we can see that the stress growth of S22 is relatively small when the module is just bent. As the bending process progresses, the stress transfer between the film layers becomes more intense, resulting in more and more intense changes in the stress experienced by the backplane. The way to solve the stress transfer is to change the OCA adhesive layer. Finally, the IS is effectively reduced by the OCA adhesive layer. This phenomenon is called the free edge effect. Furthermore, IS is singular at the free edge of the laminate. When the finite element method is used to analyze IS, the thinner the mesh near the edge, the greater the stress value

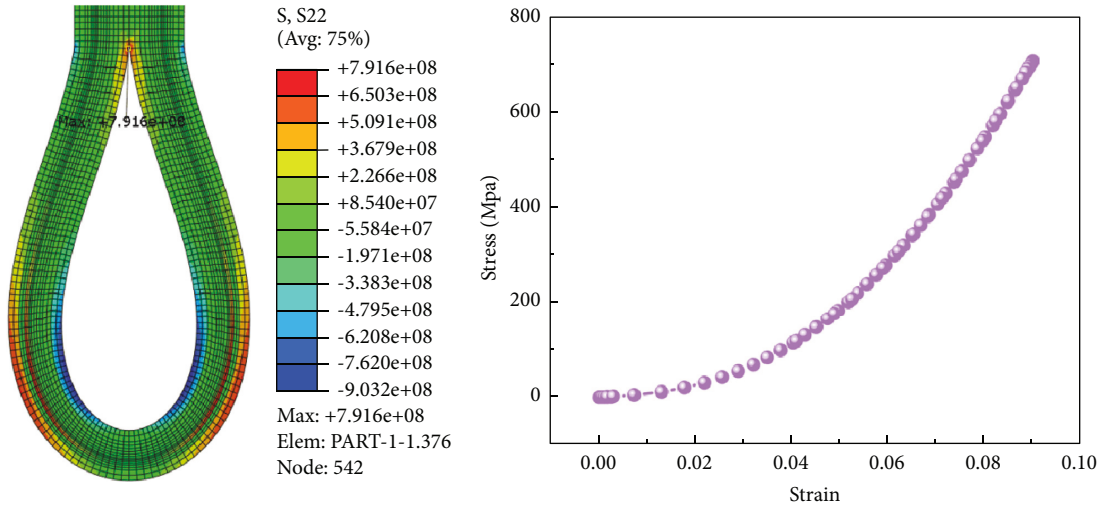

Figure 8: (a) Place where the stress of the water drop bend model s22 is the greatest and (b) the stress and strain diagram of the module at the maximum point of S22.

within the layer, until infinity. Given the relatively weak internal strength of the laminate, it is likely that the decontamination and delayering at the free edge caused the premature failure and the inability to exert its original load-bearing capacity. The classical laminate theory commonly used in engineering is based on Kirchhoff's hypothesis that each single-layer plate in the composite laminate is in a plane stress state, only in-machine stress is considered and interlayer shear strain is not considered. However, this assumption is only valid in areas far from the free edge. The fault load of the composite laminate based on this theory is usually greater than the actual load measured in the experiment, which may be caused by local interlayer pressure. Therefore, it is of great engineering practical significance to study the size and distribution of IS for predicting the final load and the displayer position and optimizing the laminate design.

4. Conclusions

An AMOLED model describing the nonlinear viscoelastic behavior of OCA is proposed. Based on the mechanical model, the IS distribution of AMOLED is discussed, and the finite element analysis of the touch layer in the folded state is performed. The bending state display module of the monitor device of the flexible panel has a plurality of neutral planes. This is because the OCA layer affects protecting each functional layer and reduces stress and strain transmission. The insignificant interaction between adjacent films can help the AMOLED device maintain relatively low pressure. The maximum longitudinal stress of the AMOLED module is at the folding symmetry, and the thickness of the OCA and the position in the module have been improved to reduce the stress and strain of the functional layer. The maximum IS in the improved module is on the protective cover, reaching 600 MPa. After exploring several dangerous locations after bending, the strain of the OCA layer is improved by 5%. The stress concentration of the module with seven neutral layers has been well improved, removing the risk of delamination or fracture.

Data Availability

The data collected and analyzed during this study are included in the paper and can also be accessed from the authors through a rational request.

Conflicts of Interest

The authors declare that they have no conflicts of interest.

Acknowledgments

This work was supported by the National Natural Science Foundation of China (22008053 and 52002111), the Key Research and Development Program of Hebei Province (20310601D and 205A4401D), and the Science Foundation of the University of Hebei Province (BJ2020053).

References

[1] K. Watanabe, Y. Iwaki, Y. Uchida, D. Nakamura, H. Ikeda, and M. Katayama, "A foldable OLED display with an in-cell touch sensor having embedded metal-mesh electrodes," *Journal of the Society for Information Display*, vol. 24, no. 1-3, pp. 12–20, 2016.

[2] Y. F. Niu, S. F. Liu, J. Y. Chiou et al., "Improving the flexibility of AMOLED display through modulating thickness of layer stack structure," *Journal of the Society for Information Display*, vol. 24, no. 5, pp. 293–298, 2016.

[3] J. Y. Chiou, Y. W. Liu, Y. F. Niu et al., "31-2: optimization of TFE structure by FTIR analysis and mechanical simulation to achieve excellent encapsulation and high flexibility AMOLED," *SID Symposium Digest of Technical Papers*, vol. 48, no. 1, pp. 437–440, 2017.

[4] H. Wang, M. Hsieh, C. Xie et al., "P-106: influence of substrate structure on the properties of flexible AMOLED displays," *SID Symposium Digest of Technical Papers*, vol. 47, no. 1, pp. 1526–1528, 2016.

[5] Y. Fujisaki, M. Nakata, Y. Nakajima et al., "47-2:*Invited paper*: oxide/organic semiconductor electronics on plastic substrates for flexible AMOLED displays," *SID Symposium Digest of Technical Papers*, vol. 47, no. 1, pp. 633–636, 2016.

[6] Q. J. Wang, W. X. Zhang, W. W. Su et al., "Influence of bending radius on the properties of flexible AMOLED displays," *Journal of the Society for Information Display*, vol. 30, no. 3, pp. 224–232, 2021.

[7] S. K. Park, J. I. Han, D. G. Moon, and W. K. Kim, "Mechanical stability of externally deformed indium–tin–oxide films on polymer substrates," *Japanese Journal of Applied Physics*, vol. 42, no. Part 1, No. 2A, pp. 623–629, 2003.

[8] S. Grego, J. Lewis, E. Vick, and D. Temple, "Development and evaluation of bend-testing techniques for flexible-display applications," *Journal of the Society for Information Display*, vol. 13, no. 7, pp. 575–581, 2005.

[9] A. Yoshida, S. Fujimura, T. Miyake et al., "21.1: invited paper: 3-inch full-color OLED display using a plastic substrate," *SID Symposium Digest of Technical Papers*, vol. 34, no. 1, pp. 856–859, 2003.

[10] M. Nishimura, K. Takebayashi, M. Hishinuma, H. Yamaguchi, and A. Murayama, "A 5.5-inch full HD foldable AMOLED display based on neutral-plane splitting concept," *Journal of the Society for Information Display*, vol. 27, 2019.

[11] M. Mizukami, N. Hirohata, T. Iseki et al., "Flexible AM OLED panel driven by bottom-contact OTFTs," *IEEE Electron Device Letters*, vol. 27, no. 4, pp. 249–251, 2006.

[12] K. Nomoto, N. Hirai, N. Yoneya et al., "A high-performance short-channel bottom-contact OTFT and its application to AM-TN-LCD," *IEEE Transactions on Electron Devices*, vol. 52, no. 7, pp. 1519–1526, 2005.

[13] D. J. Gundlach, T. N. Jackson, D. G. Schlom, and S. F. Nelson, "Solvent-induced phase transition in thermally evaporated pentacene films," *Applied Physics Letters*, vol. 74, no. 22, pp. 3302–3304, 1999.

[14] O. Hiroki, S. Toshinari, N. Kousei, I. Shunichi, S. Miyuki, and T. Yayoi, *21.3: 4.0 In. QVGA AMOLED Display Using In-Ga-Zn-Oxide TFTs with a Novel Passivation Layer*, Blackwell Publishing Ltd, Hoboken, NY, USA, 2009.

[15] J. Y. Kwon, K. S. Son, S. J. Ji, T. S. Kim, M. K. Ryu, and K. B. Park, *Bottom-Gate Gallium Indium Zinc Oxide Thin-Film Transistor Array for a High-Resolution AMOLED Display*, IEEE Electron Device Letters, Piscataway, NJ, USA, 2008.

[16] R. Keerthiwansa, J. Javorik, J. Kledrowetz, and P. Nekoksa, "Elastomer testing: the risk of using only uniaxial data for fitting the Mooney-Rivlin hyperelastic-material model," *Materiali in Tehnologije*, vol. 52, no. 1, pp. 3–8, 2018.

[17] M. Sasso, G. Palmieri, G. Chiappini, and D. Amodio, "Characterization of hyperelastic rubber-like materials by biaxial and uniaxial stretching tests based on optical methods," *Polymer Testing*, vol. 27, no. 8, pp. 995–1004, 2008.

[18] A. D. Drozdov and J. D. Christiansen, "Constitutive equations in finite elasticity of swollen elastomers," *International Journal of Solids and Structures*, vol. 50, no. 9, pp. 1494–1504, 2013.

[19] A. K. Suraj, P. Bikas, and K. Kaushik, "Effect of change of material model in Mooney Rivlin hyper-elastic material-ScienceDirect," *Materials Today: Proceedings*, vol. 26, 2020.

[20] R. Keerthiwansa, J. Javořík, S. Rusnáková, J. Kledrowetz, and P. Gross, "Hyperelastic material characterization: how the change in mooney-rivlin parameter values effect the model curve," *Materials Science Forum*, vol. 994, pp. 265–271, 2020.